RF POWER COUPLER PERFORMANCE AT CESR AND STUDY OF A MULTIPACTOR INHIBITED COUPLER*

E. Chojnacki† and S. Belomestnykh
CORNELL UNIVERSITY, Ithaca, NY, USA

Abstract

CESR has undergone a phased upgrade to replace its four NRF cavities with four SRF cavities. Details of configuration of the coupler and experience with coupling high RF power to the SRF cavities are presented. Discussions of conceptual details regarding an untried processing technique and a coupler geometry that shows promise of being less susceptible to multipactor resonances are also presented.

1 INTRODUCTION

The SRF upgrade to the CESR electron/positron storage ring at Cornell has proceeded in a phased manner for the past several years as part of a machine-encompassing luminosity upgrade.[1] CESR's four multi-cell copper NRF cavities have been replaced by four single-cell niobium-sheet SRF cavities with parameters as given in Table I. The CESR III upgrade goal is to attain 1 Amp total beam current and luminosity 1.7×10^{33} $cm^{-2}s^{-1}$.

As is becoming commonplace with SRF installations world-wide, coupling high RF power to the CESR SRF B-cells has required diligent processing of the coupler. Degradation in coupled power of about 10% occurs after several months of running, regardless of re-processing efforts, cured only by a warm up of the cryostat to evaporate accumulated condensed gases. Coupled power limits are established by the level at which repeatable vacuum bursts occur in the waveguide region, causing a dump of stored beam. Once the window is conditioned without beam, photomultiplier arc detectors viewing the vacuum side of the ceramic rarely show the window as the cause of such vacuum bursts. This indicates the discharges occur further along the waveguide during CESR operation, as described in the next section.

In the following sections, brief accounts are given of coupler layout, processing techniques, and attained power delivery to CESR beam. References are made to details which have been largely presented elsewhere. This is followed by discussions of conceptual details regarding an untried processing technique and a coupler geometry that shows promise of being less susceptible to multipactor resonances.

HOM coupling to the CESR B-cells is by way of the beampipe to room temperature beamline loads. Details of the CESR HOM loads have been reported in Ref. [2].

Table 1: Parameters of the Cornell B-cell SRF cavity.

Frequency	500 MHz
Aperture	24 cm
Effective gap	30 cm
Gradient	> 6 MV/m
Unloaded Q_o at 6 MV/m gradient	$> 10^9$
Q_{ext}	2×10^5
Shunt Impedance R	89 GΩ
Delivered power at 1 Amp beam current	325 kW
HOM power at 1 Amp beam current	13.7 kW
Number of cavities in CESR	4

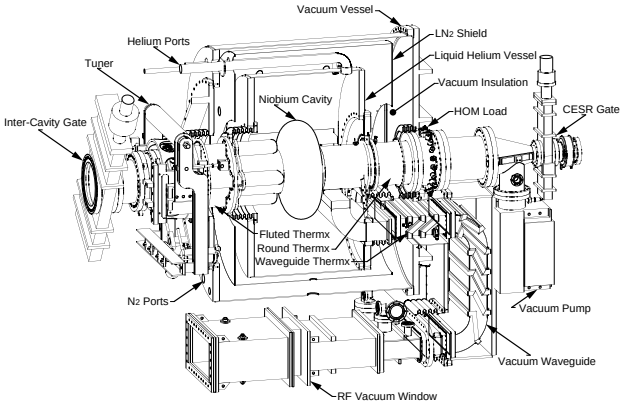

Figure 1: Layout of the CESR Mark II cryomodule.

2 COUPLER LAYOUT

As shown in the CESR SRF cryomodule layout in Fig. 1, 500MHz RF power is delivered via WR1800 air-filled rectangular waveguide to a room temperature vacuum window located beneath the cryostat. The window incorporates a transition to reduced height waveguide. A vacuum pumping section follows the window, containing photomultiplier arc detectors that view the vacuum side of the ceramic window. The pumping section is followed by a LN_2-cooled 4"×17" rectangular waveguide double-E bend, a cold He gas cooled ($\approx$ 4.5K inlet) thermal transition to the Helium vessel, then the niobium 4"×17" waveguide up to the cavity iris coupler.

The great majority of vacuum bursts which trip CESR interlocks, terminate RF, and dump beam are detected at the vacuum pumping section beneath the cryostat. As

* Work supported by the National Science Foundation.
† E-mail: epc1@cornell.edu

mentioned in the Introduction, signals from photo-multiplier arc detectors directly viewing the ceramic window rarely accompany such vacuum trips, though they do so prodigiously during unattached window processing. It is then very likely that the discharges are occurring in the double-E bend, thermal transition to the Helium vessel, and/or the niobium waveguide.

An obvious discharge culprit that SRF couplers have in common world-wide is condensed gases in the cold regions enhancing the surface secondary electron emission coefficient. This is independent of geometry and makes familiar multipactor barriers more virulent. Aggressive vacuum baking and high pumping conductance where feasible are practices given greater attention in evolving designs.

To make matters more challenging in the CESR coupler, about a meter of the interior of the double-E bend is corrugated with a sharp 1/16" sawtooth pattern as shown in Fig. 2. This was implemented to attenuate IR radiation propagating to the helium vessel and possibly deter multipacting by spoiling resonant conditions. However, the array of electric field near-singularities may be acting as emitters and generously seeding the multipactor barriers encountered. The fifth CESR cryomodule being fabricated to serve as a spare will eliminate these corrugations and further have the double-E bend made from smooth copper sheet rather than copper-plated stainless steel.

3 COUPLER PROCESSING

The challenge to SRF coupler processing is due to the characteristic of SRF cavities being greatly overcoupled without beam. The greatly overcoupled condition results in negligible traveling wave power, allowing standing-wave processing of only narrow regions of the waveguide at the standing wave's electric field crests. Indeed, vacuum trips in the CESR B-cell couplers occur at strictly repeatable traveling-wave power thresholds as beam loading increases.[3]

The most successful processing technique for the CESR B-cells has been pulsing the cavity with high RF power on or close to resonance to the point it is in the process of quenching. The RF coupling then gets close to matched and there develops a significant traveling wave component sustained for ≈ 10 ms. For pulses in which the cavity does not quench, upon termination of the RF the cavity dumps its stored energy to the waveguide. This produces a large spike of traveling wave power in the opposite direction with amplitude four times the terminated incident power.[4,5]

CESR cryomodules successive to the first have had their coupler regions modified to: 1) increase conductance in the pumping section, 2) dull the sharp ridges in the double-E bend by acid etching, and 3) include a vacuum bake of as many components as possible, even if they are subsequently exposed to atmosphere during assembly.

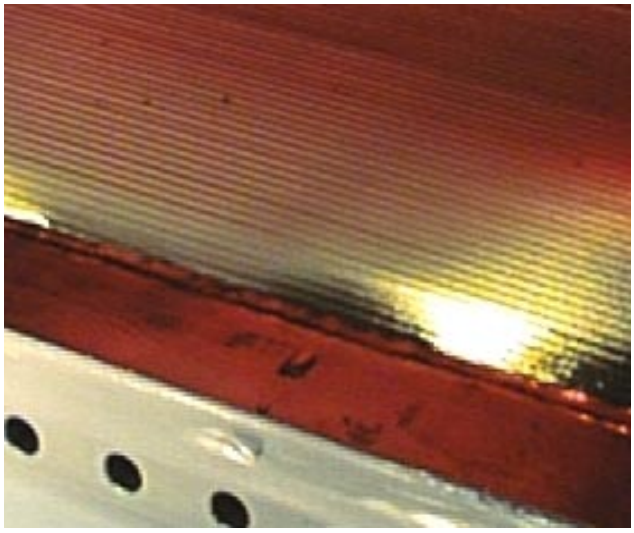

Figure 2: Photo of sawtooth pattern on interior of the double-E bend.

Considerable progress in traveling wave power has been made since the first barrier at 90 kW made itself apparent in the first CESR SRF cavity installed in Fall 1997. To date, among the three SRF cavities that have operated in CESR's East and West RF stations, the maximum power coupled to beam has been E2=212 kW, E1=218 kW, and W1=261 kW.

The W1=261 kW level was accomplished during a short run in Spring 1999, partly enabled by having the full power from a dedicated klystron available for pulse processing of the coupler. With the CESR run commencing in Fall 1999, each of the two East SRF cavities will have a dedicated 500 kW RF source rather than the previous 3dB split from a single klystron. And the fourth and final SRF cavity is now installed in station W2, sharing its feed with W1 via a 3dB split, though powered by a new 800 kW klystron which should not limit pulse processing ability. The CESR phase III luminosity goal of 1.7×10^{33} $cm^{-2}s^{-1}$ will require 325 kW to be coupled to the beam by each of the four SRF cavities.

4 WINDOW PROCESSING

Initial processing of the room temperature waveguide vacuum window occurs "offline" with two windows back-to-back as described in Refs. [5,6], up to a power of 450 kW. Much attention had been given to the nominal 30 Å titanium anti-multipactor coating on the ceramic; too thin a coating resulting in lengthy offline processing, too thick a coating causing overheating of the ceramic. In-situ operational experience with arc detectors has shown, however, that the window is rarely the cause of coupler vacuum trips, even with a thin titanium coating. Thus it is best to err on the side of too thin a titanium coating and accept lengthy offline processing, having the benefit of high power operation without concern of overheating the ceramic. Next generation higher power

window designs [7] will most likely utilize a low-loss anti-multipactor coating such as titanium oxide or chromium oxide, allowing generous thickness with little regard to overheating.

An important aspect of the window turned out to be smoothness of the copper-plated steel waveguide housing. The first three windows delivered had pinprick protrusions on the surface which would snag a clean-room cloth when wiped. During offline back-to-back processing, signals from photomultipliers viewing the vacuum side of the windows showed much greater light activity in the windows with pinpricked wall plating than windows with smooth plating.

When installed on the SRF cavity, the window ceramic is located near an electric field standing wave maximum established in an unloaded coupler. The pulse processing described in Section 3 then serves nicely to process the window ceramic region. This is confirmed by significant window arc detector activity when re-processing after the atmospheric exposure that occurs during final cryostat assembly.

In addition to offline processing of the vacuum window, future offline processing may include all coupler components up to the niobium waveguide attached to the cavity.

5 SLIDING-SHORT PROCESSING

An untried technique to process an SRF coupler in-situ is to create a cavity from the waveguide feed. Using a sliding short upstream of the window as one end of the "coupler cavity", the overcoupled SRF cavity iris then serves as the other shorted end. As the sliding short translates, an RF system must track the resonant frequency of this coupler cavity. The peak electric fields in the standing wave then scan over all but the last two or so half-periods in the coupler, as illustrated in Fig. 3, processing emitters away. A loop antenna on the face of the sliding short remains coupled to the fixed boundary condition of the B_x field of the TE_{10p} coupler mode at all times. For coax couplers, an analogous coax sliding short or rectangular-coax transition could be used.

Most of such sliding-short processing takes place at frequencies removed from the SRF cavity's accelerating mode, processing multipactor resonances that are different from those encountered during SRF cavity operation. The general effect of burning off high field emitters, though, eliminates them as sources for all resonances. Additionally, bombardment of coupler surfaces during such processing "scrubs" them to lower their secondary emission coefficient.

For a rectangular waveguide coupler of width a and height b, the peak TE_{10} traveling wave electric field along the centerline is given by

$$E_o = \sqrt{\frac{4PZ_{TE}}{ab}} \quad , \qquad (1)$$

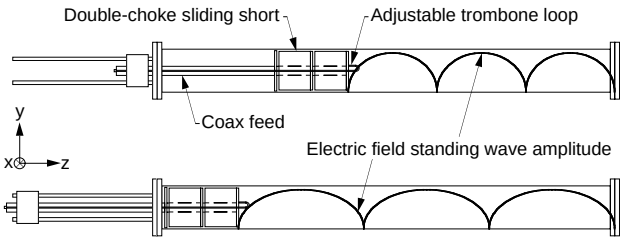

Figure 3: Sliding-short manipulation of a standing wave in a coupler to scan the peak electric fields over the surfaces.

where P is the traveling wave power,

$$Z_{TE} = \frac{\eta_o}{\sqrt{1-\left(ck_c/\omega\right)^2}} \qquad (2)$$

is the guide wave impedance, η_o the free space impedance, c the speed of light, $k_c = \pi/a$, and ω the angular frequency. Viewing the coupler as a cavity of length d being processed in the TE_{10p} mode, the dissipated wall power in terms of the standing-wave peak electric field E_o along the centerline is given by

$$W_L = \frac{R_s E_o^2}{2\omega_r{}^2\mu_o^2}\left[k_c^2\left(bd+\frac{ad}{2}\right)+k_z^2\left(ab+\frac{ad}{2}\right)\right] \quad , \qquad (3)$$

where R_s is the wall surface resistivity, ω_r the resonant angular frequency that must satisfy

$$\omega_r = c\sqrt{k_c{}^2 + k_z{}^2} \quad , \qquad (4)$$

μ_o the permeability of free space, and $k_z = p\pi/d$.

The CESR SRF coupler has $a = 43.18$ cm and $b = 10.16$ cm. From eq. (1) the phase III target of 325 kW traveling wave delivered to beam at 500 MHz corresponds to a peak TE_{10} electric field of $E_o = 125$ kV/m. Using a practical axial mode number of $p = 8$ and surface resistivity R_s corresponding to room temperature copper, eq. (3) gives 291 W required to generate $E_o = 125$ kV/m at 500 MHz and cavity length $d = 3.33$ m. This increases to 370 W at 444 MHz when the sliding short is retracted 1 m. Solid state RF sources are readily available with such powers and frequency range.

In the CESR SRF coupler, however, the copper plating on the stainless steel walls is rather poor. Taking the surface resistivity as that of steel, the TE_{108} powers increase to 2.1 kW at 500 MHz and 2.7 kW at 444 MHz. Solid state RF sources are also available at these powers, but the cost is quite high.

Sliding-short standing-wave processing may prove to be an effective way to process nearly all regions of SRF couplers in-situ. It will require temporarily breaking the RF feed upstream of the vacuum window and installing the sliding-short apparatus. If the coupler is fabricated with quality copper surfaces, the TE_{10p} cavity power required to establish the equivalent electric field of TE_{10} traveling-wave operation is reasonable.

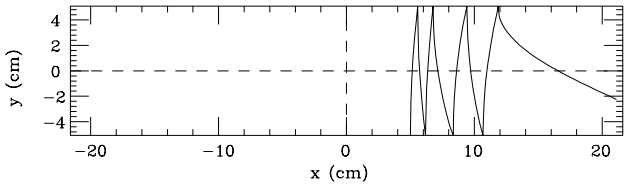

Figure 4: Trajectory of an electron launch displaced from the midline in the TE_{10} mode of rectangular waveguide.

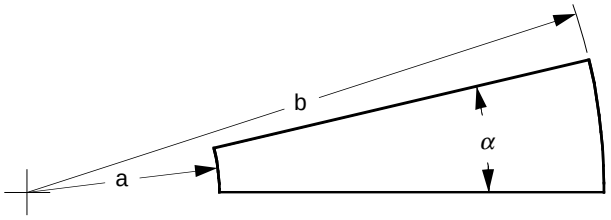

Figure 5: Wedge-shaped hollow waveguide cross section.

6 NOVEL COUPLER GEOMETRY

Over two decades ago, implementation of a rounded SRF cavity profile [8] instead of pillbox enabled suppression of many virulent multipactor resonances which had severely hindered SRF cavity performance up to that time. A similar geometrical approach to SRF coupler variation is presented here.

Electron trajectory tracking codes have long successfully quantified multipactor resonances.[9] In rectangular waveguide, TE_{10} mode 2-point multipactor resonances have been shown to occur along the cross-sectional midline at the peak of the electric field. These multipactor barriers visualized by 2D simulation agree well with experiment.[10] Using the rectangular waveguide TE_{10} convention of E_y, B_x, and B_z, these resonances also have slow migration along the z-axis arising from the $v_y \times B_x$ Lorentz force. Interestingly, trajectories launched displaced from the midline experience a transverse $v_y \times B_z$ force and migrate to the sidewall after a few impacts, as shown in Fig. 4. There the electric field is zero and successive low energy impacts quickly damp secondary multiplication to negligible levels.

For coaxial couplers with aligned, round conductors, troublesome TEM mode resonances have been shown to typically occur with repeating impacts on the outer conductor wall. Again, trajectories closely follow the radial electric field and have slow migration along the axis arising from the $v_r \times B_\theta$ Lorentz force. Coax multipactor barrier power levels predicted by 2D simulation agree well with experiment.[11,12]

Since both rectangular and coaxial waveguide multipactor trajectories remain well aligned with the respective mode's electric field, a resonance-disrupting effect may be provided by altering the waveguide cross section so as to force a curvature on the electric field. This could disallow the trajectories from traversing repeatable paths and even drive them to regions of zero electric field.

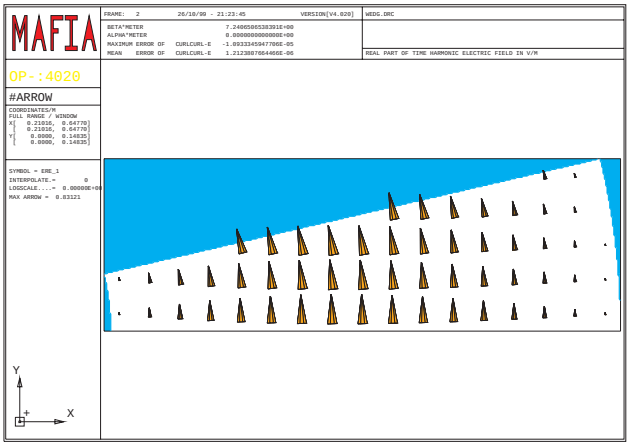

Figure 6: MAFIA solution of the electric field of the fundamental mode of the waveguide illustrated in Fig. 5.

One such unconventional waveguide cross section is illustrated in Fig. 5. Rectangular waveguide is altered to have the broad walls non-parallel and the sidewalls as circular arcs to facilitate analysis. This "wedgeguide" has a fundamental mode similar to the rectangular TE_{10}. Modifications to coax have been explored elsewhere [13,14], but since TEM modes have no region of zero electric field, resonant trajectories remained. Discussion of the wedge-shaped hollow waveguide follows.

6.1 Wedgeguide

A MAFIA solution of the electric field of the fundamental mode of the waveguide illustrated in Fig. 5 is shown in Fig. 6. This mode can be analytically treated as a higher order TE mode of coaxial waveguide where the broad walls are on $\theta = const$ surfaces and the sidewalls are on $r = const$ surfaces, as indicated in Fig. 5. The azimuthal harmonic of this TE mode is $n = 0$ and the cutoff wavenumber k_c is given by solution of the transcendental equation

$$\frac{J_o'(k_c a)}{J_o'(k_c b)} = \frac{N_o'(k_c a)}{N_o'(k_c b)} \quad , \tag{5}$$

where J and N are the usual Bessel functions.[15] The field components are given by

$$E_\theta = E_o\left[J_1(k_c r) - gN_1(k_c r)\right]\mathrm{e}^{j(\omega t - \beta z)} \tag{6a}$$

$$H_r = \frac{-\beta E_\theta}{\omega\mu} \tag{6b}$$

$$H_z = \frac{-jk_c E_o}{\omega\mu}\left[J_0(k_c r) - gN_0(k_c r)\right]\mathrm{e}^{j(\omega t - \beta z)} \tag{6c}$$

where

$$g \equiv \frac{J_1(k_c a)}{N_1(k_c a)} \quad . \tag{7}$$

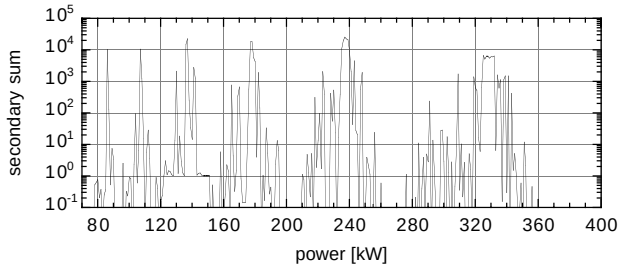

Figure 7: Secondary multiplication in CESR rectangular waveguide after 20 impacts.

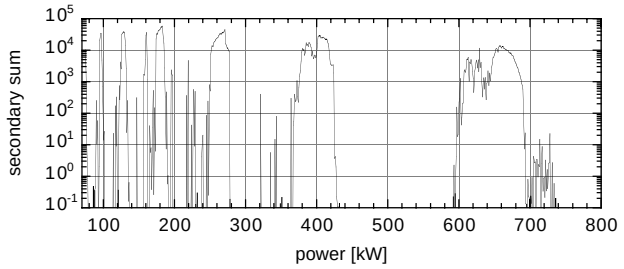

Figure 8: Secondary multiplication in TESLA 40 mm 50 Ω coax after 20 impacts.

The peak azimuthal electric field occurs at a radius r_e solving

$$J_0(k_c r_e) - \frac{J_1(k_c r_e)}{k_c r_e} - g\left[N_0(k_c r_e) - \frac{N_1(k_c r_e)}{k_c r_e} \right] = 0 \qquad (8)$$

and has the value

$$E_{\theta\ peak} = E_o\left[J_1(k_c r_e) - g N_1(k_c r_e) \right] \quad . \qquad (9)$$

Integration of the Poynting vector gives the propagating power as

$$P = \frac{\alpha E_o^{\ 2} \beta}{4\omega\mu}\left[r^2\left(R_1^{\ 2}(k_c r) - R_0(k_c r) R_2(k_c r) \right) \right]_a^b \quad , \qquad (10)$$

where

$$R_n(x) \equiv J_n(x) - g N_n(x) \quad . \qquad (11)$$

These analytic forms allow greater accuracy and computation speed of a trajectory code than using, e.g., interpolation of MAFIA fields shown in Fig. 6.

6.2 Multipactor Code

A code was written to search for multipactor resonances in 2D geometry. Electrons are launched from a range of selected locations at a range of RF phases, typically -30˚ to 180˚ in 5˚ steps with the electric field $E \propto \sin(\phi)$. The RF power is scanned over a selected range in 1 kW steps. For each RF launch phase at each power level, secondary electron multiplication due to impacts is logged by a multiplicative counter utilizing a familiar curve of secondary yield vs. impact energy.[16] At each power level these secondary multiplications are summed over all launch phases. This is similar to what has been termed an

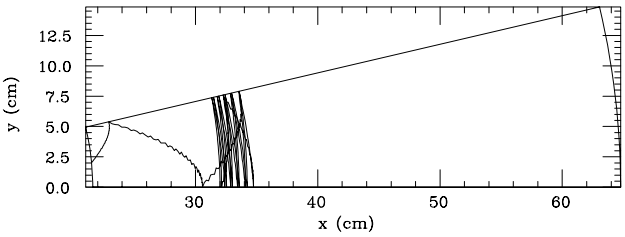

Figure 9: Trajectory of an electron launched at 32 cm in wedgeguide and experiencing a short term transverse force balance, eventually migrating to a sidewall.

"enhanced counter function," except there are no restrictions decided by RF phase upon secondary launch.[11,17] The initial electron and all secondaries are launched at 2 eV normal to the surface. The code is typically run for 20 impacts per initial launch condition, terminated if secondary multiplication becomes $< 10^{-3}$, or terminated if the electron hits a specified boundary, such as a rectangular waveguide sidewall.

As a test of the code it was run for known simulated and experimental cases of rectangular and coaxial waveguide.[10,12] The results are shown in Fig. 7 for CESR rectangular waveguide and in Fig. 8 for TESLA 40 mm 50 Ω coax. These agree well with previous simulations and experiments.

6.3 Wedgeguide Multipactor Simulations

The traveling-wave RF fields in eq. (6) were used in the above described multipactor code. Three phenomenon in wedgeguide have become apparent after initial scans of RF power, launch phase, and launch position:

1) The great majority of electron trajectories alternately impacting on the broadwalls quickly become anti-resonant with the RF. After a dozen or so impacts they perform successive low energy impacts and secondary multiplication quickly decays to negligible values.
2) The trajectories have a migration bias toward the larger radius sidewall due to the E_θ field curvature. Trajectories that survive anti-resonant conditions well enough to maintain a significant secondary multiplication migrate to this wall and are assumed to terminate there, just as seen with normal rectangular waveguide.
3) The outward radial migration due to the E_θ field curvature opposes the net inward radial $v_\theta \times B_z$ force that occurs at radii less than the peak of the E_θ field as given by eq. (8). For several RF power levels these opposing forces are close to equal and the electron trajectory can remain close to resonant in an $r = const$ vicinity. Fortunately, for all such cases revealed to date, the force balance is not constant along the trajectory and it eventually becomes anti-resonant and/or migrates to a sidewall after a couple dozen impacts, as shown in Fig. 9. The secondary

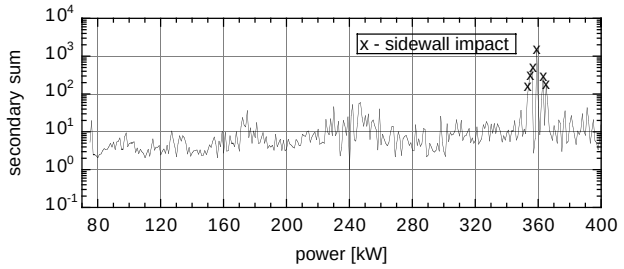

Figure 10: Secondary multiplication in wedgeguide after 20 impacts with initial electron launch position at 32 cm. The ×'s correspond to the short term balanced trajectories described in item 3 above which terminate at a sidewall.

multiplication function may be high upon sidewall impact, but it is assumed that having zero electric field there causes successive low energy impacts to quickly damp secondary multiplication to negligible levels.

The departure from resonance described in item 3 is in contrast to standard rectangular waveguide multipactor resonance along the centerline. Rectangular centerline resonances are fairly stable since there is a smooth null in the B_z field there. Secondary multiplication simply increases ad infinitum as number of allowed impacts increases. If the wedgeguide is altered to have flat sidewalls rather than radiused, the mild radial force balance described in item 3 may be further disturbed so as to decay even faster.

Shown in Fig. 10 is secondary multiplication vs. power for wedgeguide with initial electron launch position at 32 cm on the lower axis shown in Fig. 9. The ×'s in Fig. 10 correspond to the short term balanced trajectories described in item 3 above. Launching at 32 cm has shown the most likelihood of experiencing short term balanced trajectories. All such trajectories were terminated in the simulation upon sidewall impact. Future simulations will continue tracking secondaries from the sidewalls to verify secondary multiplication decaying to negligible levels there.

Thus far the wedgeguide geometry shows promise as having greatly reduced multipactor susceptibility. A coupler fabricated with this shape would likely still require some processing to burn off emitters, but it is hoped that such processing will proceed quicker and not show degradation as experienced with current couplers. Care would also have to be taken to ensure there are no other multipactor-susceptible components in the coupler chain, such as the vacuum window. Window designs with no electric field components normal to the ceramic would keep stray electrons from impacting these typically high secondary coefficient materials.[5]

7 ACKNOWLEDGEMENT

The support provided by R. Kaplan, P. Quigley, J. Reilly, and CESR operators throughout SRF commissioning has been indispensable.

8 REFERENCES

[1] D.L. Rubin, "Results of the CESR upgrade," *Proc. 6th European Part. Accel. Conf.*, Stockholm, (1998).

[2] E. Chojnacki and W.J. Alton, "Beamline RF Load Development at Cornell," *Proc. 1999 Part. Accel. Conf.*, New York, NY, 845 (1999).

[3] Observed by S. Belomestnykh during CESR machine studies.

[4] S. Belomestnykh, *et al.*, "Commissioning of the superconducting RF cavities for the CESR luminosity upgrade," *Proc. 1999 Part. Accel. Conf.*, New York, NY, 980 (1999).

[5] E. Chojnacki, *et al.*, "Tests and designs of high-power waveguide vacuum windows at Cornell," *Part. Accel.* **61**:[309]45 (1998).

[6] M. Pisharody, *et al.*, "High power tests on a 500 MHz planar waveguide window for the CESR upgrade," *Proc. 1995 Part. Accel. Conf.*, Dallas, TX, 1720 (1995).

[7] E. Chojnacki, *et al.*, "Design of a high average-power waveguide window," *Proc. 1997 Part. Accel. Conf.*, Vancouver, B.C., 3177 (1997).

[8] V. Lagomarsino, G. Manuzio, R. Parodi, and R. Vaccarone, "Measurements on niobium superconducting C band cavities for linear accelerators applications," IEEE Trans. Magn. **MAG-15** (1), 25-26 (1979).

[9] U. Klein and D. Proch, "Multipacting in superconducting RF structures," *Proc. Conf. Future Possibilities for Electron Accel.*, ed. J.S. McCarthy and R.R. Whitney (U. Virginia, Charlottesville, VA, 1979) pp. N1-17.

[10] R.L. Geng and H.S. Padamsee, "Exploring multipacting characteristics of a rectangular waveguide," *Proc. 1999 Part. Accel. Conf.*, New York, NY, 429 (1999).

[11] E. Somersalo, P. Yla-Oijala, and D. Proch, "Analysis of multipacting in coaxial lines," *Proc. 1995 Part. Accel. Conf.*, Dallas, TX, 1500 (1995).

[12] B. Dwersteg, "High power windows at DESY," *Proc. 8th Workshop on RF Superconductivity*, ed. V. Palmieri and A. Lombardi (Abano Terme, Italy, 1997), pp. 740-752.

[13] J. Tuckmantel, "Reduction of multipacting with an eccentric coaxial coupler," CERN LEP2 Note 94-25 (1994).

[14] J. Tuckmantel, "Improvements to power couplers for the LEP2 superconducting cavities," *Proc. 1995 Part. Accel. Conf.*, Dallas, TX, 1642 (1995).

[15] S. Ramo, J.R. Whinnery, and T. Van Duzer, *Fields and waves in communication electronics*, 3rd ed. (Wiley, New York, 1994) pp. 433-435.

[16] H.Piel, "Superconducting cavities", *Proc. CERN Accel. School, Superconductivity in Part. Accel.*, ed. S. Turner (Haus Rissen, Hamburg, 1988), CERN 89-04, p. 176.

[17] E. Somersalo, *et al.*, "Computational methods for analyzing electron multipacting in RF structures," *Part. Accel.* **59**, 107 (1998).